JTE
HCMUTE
ISSN: 2615-9740

JOURNAL OF TECHNICAL EDUCATION SCIENCE
Ho Chi Minh City University of Technology and Education
Website: https://jte.edu.vn
Email: jte@hcmute.edu.vn

Free Vibration of the Magneto-Electro-Elastic Plates Resting on Elastic Foundation Using the Refined Plate Theory with Two Variables

L. T. Phong[1], T. Nguyen-Thanh[2], N. A. Dat[1], T. T. Trien[1], P. T. Hung[1,*]
[1]*Ho Chi Minh City University of Technology and Education, Vietnam*
[2]*Ho Chi Minh City University of Technology (HUTECH), Vietnam*

[*] Corresponding author. *Email: hungpht@hcmute.edu.vn*

ARTICLE INFO

Received: 19/06/2023
Revised: 29/06/2023
Accepted: 06/07/2023
Published: 28/08/2024

KEYWORDS

Free vibration;
Functionally graded magneto-electro-elastic plate;
Isogeometric analysis;
Refined plate theory;
Elastic foundation.

ABSTRACT

The objective of this article is to investigate the free vibration analyses of the functionally graded magneto-electro-elastic (FG MEE) plates supported by an elastic foundation using the refined plate theory (RPT) with two variables. The elastic foundation is modeled utilizing the Winkler-Pasternak theory. The power-law model is employed to characterize the graded material properties of the FG MEE plates. According to the RPT and Hamilton's principle, the governing equations of the FG MEE plate are derived. The displacement fields and electric and magnetic potentials are approximated using the Non-Uniform Rational B-Splines (NURBS) basic functions of the isogeometric approach (IGA). The proposed model's advantages and accuracy are demonstrated by comparing the obtained results with those reported in the existing literature. The study comprehensively examines and discusses the impact of several parameters, including the power index, initial external magnetic potential and electric voltage, and the geometry, on the vibration frequency of the FG MEE plates. The numerical findings indicate that an increase in the power index leads to a decrease in the frequency of the FG MEE plates. Besides, the stiffness of FG MEE plates decreases with an increase in the initial external electric voltage, whereas it increases with an increase in the initial external magnetic potential. This article presents valuable perspectives on examining vibration analysis of the FG MEE plates, which can inform the design of innovative materials and structures with customized properties.

Doi: https://doi.org/10.54644/jte.2024.1424

1. Introduction

Magneto-electro-elastic materials are a class of smart materials that exhibit combined ferromagnetic, piezoelectric, and dielectric properties. These materials have garnered significant interest because they can react to various external stimuli, including magnetic fields, electric fields, and mechanical stress. Integrating these properties within a single material enables MEE materials to perform various functions, such as sensing, actuation, energy conversion, and control. The controllable and tunable response of MEE materials to external fields and stress makes them attractive for various applications, including smart structures, actuators, sensors and energy harvesting systems. Due to the advantages and wide-ranging applications of MEE materials, researchers have dedicated significant attention to analyzing the behavior of beam, plate, and shell structures constructed from this material. Pan [1] successfully obtained the exact solution for orthogonal 3D plates and multilayer plates subjected to static loads composed of linear MEE materials. The free vibration of the multilayer MEE plate was presented by Ramirez et al. [2] using the Ritz solution. Moita et al. [3] addressed free vibration and static bending

responses of MEE plates with the aid of the finite element method (FEM) according to the high-order shear deformation theory (HSDT). In addition, Badri et al. [4] also employed the analytical approach to analyze the MEE plates under the thermal load. The HSDT and higher-order FEM were utilized by Vinyas et al. [5] to investigate the static bending of the sandwich plates made of piezomagnetic and piezoelectric materials in hygral and thermal environments. Besides, Shooshtari et al. [6] also used the first-order shear deformation theory (FSDT) to study the analytical vibration with a large amplitude of the multilayer MEE plate resting on an elastic foundation. Employing the nonlocal strain gradient theory (NSGT), Malikan et al. [7] introduced the buckling of the MEE nanoplates under hygral and thermal loads.

Functionally graded materials (FGMs) have demonstrated the capability to mitigate stress concentration at the interfaces between layers, a common issue in traditional composites. As a result, structures constructed with functionally graded materials have found extensive applications in various fields such as mechanics, construction, aviation, and space industries. In recent years, researchers have been interested in investigating the mechanical behavior of structures composed of FG MEE material. Numerous scientists have studied this area, aiming to better understand the performance and potential applications of FG MEE-based structures. Specifically, the Pagano method is employed by Wu et al. [8], [9] to study static and vibration behaviors of the multilayer FG MEE plate. The analytical solution of the buckling response of the FG porous MEE plate was found by Ebrahimi et al. [10] according to the RPT and analytical approach. On the other hand, Ni et al. [11] investigated the analytical free vibration of cylindrical shells made of FG MEE material according to the Reissner shell theory. The moving least-squares method was used by Sladek et al. [12] to find the solution to the static bending of the FG MEE circular plate. The analytical free vibration of the sandwich plate with the FG MEE face sheets was presented by Ebrahimi et al. [13] employing the RPT.

The literature review indicates that previous studies on MEE structures predominantly relied on analytical methods suitable for addressing simpler problems with simple boundaries. However, numerical methods such as the FEM, meshfree method, and IGA are considered the most appropriate and effective approaches when dealing with complex boundary conditions. These numerical methods provide greater versatility and accuracy in handling intricate boundary configurations and offer valuable insights into the behavior of the FG MEE structures under complex conditions. The IGA technique can efficiently capture higher-order derivatives inherent in the RPT. This is attributed to its foundation in NURBS basis functions, which offer exceptional versatility in achieving the desired level of continuity within the basis functions. Hughes [14] was the first to propose the IGA and its associated computational expense. According to the IGA, the mechanical responses of the FG plates [15], [16], microplates [17], [18] and nanoplates [19], [20] were investigated recently. The literature reviewed above reveals that there have been no investigations into the free vibration response of FG MEE supported by the Winkler-Pasternak foundation utilizing a combination of the RPT incorporating two variables and IGA. This paper addresses the research gap by employing the RPT with two variables and IGA to introduce the free vibration of the FG MEE plates under the initial external electric voltage and magnetic potential. The influence of various factors, including power index, external electric and magnetic loads, spring and shear coefficients of an elastic foundation and geometric parameters on the natural frequency of the FG MEE plates is analyzed and discussed.

2. The basic equations

2.1. The RPT with two variables

Consider the FG MEE rectangular and circular plates with the thickness *h*, as shown in Figure 1. With the aid of the RPT with two variables [21], the components of the displacement vector of the FG MEE plate are defined by

$$\begin{cases} \tilde{u}(x,y,z) = -zw_{b,x}(x,y) + f(z)w_{s,x}(x,y) \\ \tilde{v}(x,y,z) = -zw_{b,y}(x,y) + f(z)w_{s,y}(x,y) \\ \tilde{w}(x,y,z) = w_b(x,y) + w_s(x,y) \end{cases} \quad (1)$$

where w_b and w_s represent the transverse displacements caused by bending and shear, respectively; symbol "," represents the differential operator; $f(z)=-4z^3/3h^2$ is the distribution function.

The Eq. (1) is reformed in matrix form by following

$$\mathbf{u}=\mathbf{u}_1+z\mathbf{u}_2+f(z)\mathbf{u}_3;\text{with}$$
$$\mathbf{u}=\begin{Bmatrix}\tilde{u}\\ \tilde{v}\\ \tilde{w}\end{Bmatrix};\mathbf{u}_1=\begin{Bmatrix}0\\ 0\\ w_b+w_s\end{Bmatrix};\mathbf{u}_2=\begin{Bmatrix}-w_{b,x}\\ -w_{b,y}\\ 0\end{Bmatrix};\mathbf{u}_3=\begin{Bmatrix}w_{s,x}\\ w_{s,y}\\ 0\end{Bmatrix} \tag{2}$$

By employing Eq. (2), the tensor of linear strain is considered by following

$$\boldsymbol{\varepsilon}=\begin{Bmatrix}\boldsymbol{\varepsilon}_b\\ \boldsymbol{\varepsilon}_s\end{Bmatrix}=\begin{Bmatrix}z\boldsymbol{\varepsilon}_{b1}+f(z)\boldsymbol{\varepsilon}_{b2}\\ \left(1+f'(z)\right)\boldsymbol{\gamma}_s\end{Bmatrix} \tag{3}$$

in which

$$\boldsymbol{\varepsilon}_b=\begin{Bmatrix}\varepsilon_x\\ \varepsilon_y\\ \gamma_{xy}\end{Bmatrix};\boldsymbol{\varepsilon}_{b1}=-\begin{Bmatrix}w_{b,xx}\\ w_{b,yy}\\ 2w_{b,xy}\end{Bmatrix};\boldsymbol{\varepsilon}_{b2}=\begin{Bmatrix}w_{s,xx}\\ w_{s,yy}\\ 2w_{s,xy}\end{Bmatrix};\boldsymbol{\varepsilon}_s=\begin{Bmatrix}\gamma_{xz}\\ \gamma_{yz}\end{Bmatrix};\boldsymbol{\gamma}_s=\begin{Bmatrix}w_{s,x}\\ w_{s,y}\end{Bmatrix} \tag{4}$$

Besides, to fulfill the requirements of Maxwell's equations, the magnetic potential Ψ and electric potential Φ are expressed as follows [22]

$$\Psi(x,y,z)=g(z)\psi(x,y)+\frac{2z}{h}\Omega_0;\Phi(x,y,z)=g(z)\varphi(x,y)+\frac{2z}{h}V_0 \tag{5}$$

where $g(z)=-\cos(\pi z/h)$ represents distributed function; V_0 is the external electric voltage, whereas Ω_0 denotes the external magnetic potential.

Employing Maxwell's equations, vectors of magnetic field (**H**) and electric field (**E**) are derived from Eq. (5) as follows

$$\mathbf{H}=\begin{Bmatrix}H_x\\ H_y\\ H_z\end{Bmatrix}=-\nabla\Psi=-\begin{Bmatrix}g(z)\psi_{,x}\\ g(z)\psi_{,y}\\ g'(z)\psi+\dfrac{2\Omega_0}{h}\end{Bmatrix};\mathbf{E}=\begin{Bmatrix}E_x\\ E_y\\ E_z\end{Bmatrix}=-\nabla\Phi=-\begin{Bmatrix}g(z)\varphi_{,x}\\ g(z)\varphi_{,y}\\ g'(z)\varphi+\dfrac{2V_0}{h}\end{Bmatrix} \tag{6}$$

in which H_x, H_y and H_z denote the magnetic field's components, while E_x, E_y and E_z represent the electric field's components.

a) Rectangular b) Circular

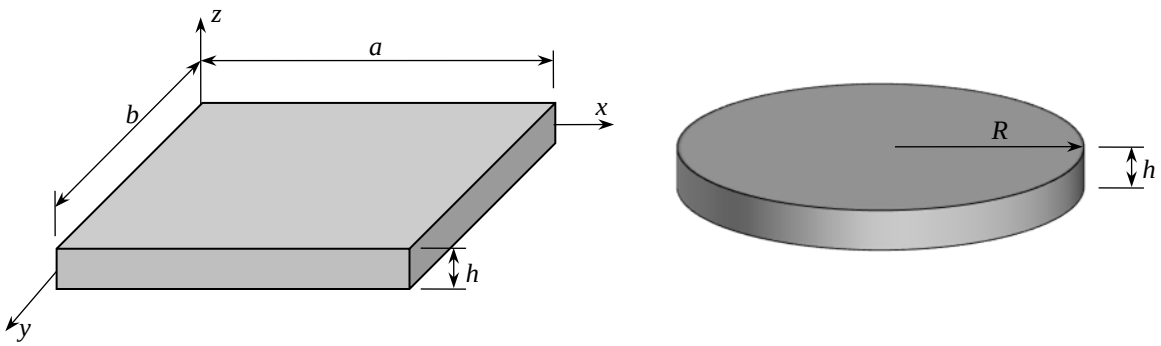

Figure 1. *The geometry of the FG MEE plates*.

2.2. The constitutive relations

The constitutive equations of the FG MEE plate considering the magneto-electro-elastic coupling are presented as follows [7], [23]

$$\begin{aligned}
&\boldsymbol{\sigma}_b = \mathbf{C}_{uub}\boldsymbol{\varepsilon}_b - \mathbf{C}_{ueb}\mathbf{E}_b - \mathbf{C}_{umb}\mathbf{H}_b; \boldsymbol{\sigma}_s = \mathbf{C}_{uus}\boldsymbol{\varepsilon}_s - \mathbf{C}_{ues}\mathbf{E}_s - \mathbf{C}_{ums}\mathbf{H}_s;\\
&\mathbf{D}_b = \mathbf{C}_{ueb}^T\boldsymbol{\varepsilon}_b + \mathbf{C}_{eeb}\mathbf{E}_b + \mathbf{C}_{emb}\mathbf{H}_b; \mathbf{D}_s = \mathbf{C}_{ues}^T\boldsymbol{\varepsilon}_s + \mathbf{C}_{ees}\mathbf{E}_s + \mathbf{C}_{ems}\mathbf{H}_s;\\
&\mathbf{B}_b = \mathbf{C}_{umb}^T\boldsymbol{\varepsilon}_b + \mathbf{C}_{emb}\mathbf{E}_b + \mathbf{C}_{mmb}\mathbf{H}_b; \mathbf{B}_s = \mathbf{C}_{ums}^T\boldsymbol{\varepsilon}_s + \mathbf{C}_{ems}\mathbf{E}_s + \mathbf{C}_{mms}\mathbf{H}_s
\end{aligned} \tag{7}$$

with

$$\begin{aligned}
&\boldsymbol{\sigma}_b = \begin{Bmatrix}\sigma_x\\ \sigma_y\\ \tau_{xy}\end{Bmatrix}; \mathbf{D}_b = \begin{Bmatrix}0\\ 0\\ D_z\end{Bmatrix}; \mathbf{B}_b = \begin{Bmatrix}0\\ 0\\ B_z\end{Bmatrix}; \boldsymbol{\sigma}_s = \begin{Bmatrix}\tau_{xz}\\ \tau_{yz}\end{Bmatrix}; \mathbf{D}_s = \begin{Bmatrix}D_x\\ D_y\end{Bmatrix}; \mathbf{B}_s = \begin{Bmatrix}B_x\\ B_y\end{Bmatrix};\\
&\mathbf{H}_b = \begin{Bmatrix}0\\ 0\\ H_z\end{Bmatrix}; \mathbf{E}_b = \begin{Bmatrix}0\\ 0\\ E_z\end{Bmatrix}; \mathbf{H}_s = \begin{Bmatrix}H_x\\ H_y\end{Bmatrix}; \mathbf{E}_s = \begin{Bmatrix}E_x\\ E_y\end{Bmatrix}
\end{aligned} \tag{8}$$

and

$$\begin{aligned}
&\mathbf{C}_{uub} = \begin{bmatrix}\bar{c}_{11} & \bar{c}_{12} & 0\\ \bar{c}_{12} & \bar{c}_{22} & 0\\ 0 & 0 & \bar{c}_{66}\end{bmatrix}; \mathbf{C}_{ueb} = \begin{bmatrix}0 & 0 & \bar{e}_{31}\\ 0 & 0 & \bar{e}_{31}\\ 0 & 0 & 0\end{bmatrix}; \mathbf{C}_{umb} = \begin{bmatrix}0 & 0 & \bar{q}_{31}\\ 0 & 0 & \bar{q}_{31}\\ 0 & 0 & 0\end{bmatrix}; \mathbf{C}_{eeb} = \begin{bmatrix}0 & 0 & 0\\ 0 & 0 & 0\\ 0 & 0 & \bar{k}_{33}\end{bmatrix};\\
&\mathbf{C}_{mmb} = \begin{bmatrix}0 & 0 & 0\\ 0 & 0 & 0\\ 0 & 0 & \bar{\mu}_{33}\end{bmatrix}; \mathbf{C}_{emb} = \begin{bmatrix}0 & 0 & 0\\ 0 & 0 & 0\\ 0 & 0 & \bar{d}_{33}\end{bmatrix}; \mathbf{C}_{uus} = \begin{bmatrix}\bar{c}_{44} & 0\\ 0 & \bar{c}_{55}\end{bmatrix}; \mathbf{C}_{ues} = \begin{bmatrix}\bar{e}_{15} & 0\\ 0 & \bar{e}_{15}\end{bmatrix};\\
&\mathbf{C}_{ums} = \begin{bmatrix}\bar{q}_{15} & 0\\ 0 & \bar{q}_{15}\end{bmatrix}; \mathbf{C}_{ees} = \begin{bmatrix}\bar{k}_{11} & 0\\ 0 & \bar{k}_{11}\end{bmatrix}; \mathbf{C}_{mms} = \begin{bmatrix}\bar{\mu}_{11} & 0\\ 0 & \bar{\mu}_{22}\end{bmatrix}; \mathbf{C}_{ems} = \begin{bmatrix}\bar{d}_{11} & 0\\ 0 & \bar{d}_{22}\end{bmatrix}
\end{aligned} \tag{9}$$

where $\sigma_x, \sigma_y, \tau_{xy}, \tau_{xz}, \tau_{yz}$ denote the stress components; B_x, B_y, B_z and D_x, D_y, D_z represent the magnetic and electric displacement components, respectively. In addition, $\bar{c}_{ij}, \bar{e}_{ij}, \bar{q}_{ij}$ and $\bar{k}_{ij}$ denote the reduced coefficients of elastic stiffness, piezoelectric, piezomagnetic and dielectric permittivity, respectively. Finally, $\bar{d}_{ij}$ and $\bar{\mu}_{ij}$ represent the reduced electromagnetic and magnetic permittivity coefficients, respectively. The formulation of the reduced material properties in Eq. (7) is presented in following forms

$$\begin{aligned}
&\bar{c}_{11} = c_{11} - \frac{c_{13}^2}{c_{33}}; \bar{c}_{12} = c_{12} - \frac{c_{13}^2}{c_{33}}; \bar{c}_{66} = c_{66}; \bar{c}_{55} = c_{55}; \bar{c}_{44} = c_{44}; \bar{e}_{31} = e_{31} - \frac{e_{33}c_{13}}{c_{33}}; \bar{e}_{15} = e_{15}; \bar{q}_{15} = q_{15};\\
&\bar{q}_{31} = q_{31} - \frac{q_{33}c_{13}}{c_{33}}; \bar{k}_{33} = k_{33} + \frac{e_{33}^2}{c_{33}}; \bar{k}_{11} = k_{11}; \bar{d}_{33} = d_{33} + \frac{q_{33}e_{33}}{c_{33}}; \bar{d}_{11} = d_{11}; \bar{\mu}_{33} = \mu_{33} + \frac{q_{33}^2}{c_{33}}; \bar{\mu}_{11} = \mu_{11}
\end{aligned} \tag{10}$$

in which the coefficients $c_{ij}, e_{ij}, q_{ij}, k_{ij}, d_{ij}$ and μ_{ij} are the FG MEE plate's effective material properties. In this article, the material properties of the FG MEE plate exhibit continuous variation across the plate thickness, following a power-law scheme. The effective material properties of the plate are expressed below [24]

$$\begin{aligned}
&c_{ij}(z) = c_{ij}^b + \left(\frac{z}{h} + \frac{1}{2}\right)^n \left(c_{ij}^t - c_{ij}^b\right); e_{ij}(z) = e_{ij}^b + \left(\frac{z}{h} + \frac{1}{2}\right)^n \left(e_{ij}^t - e_{ij}^b\right)\\
&q_{ij}(z) = q_{ij}^b + \left(\frac{z}{h} + \frac{1}{2}\right)^n \left(q_{ij}^t - q_{ij}^b\right); k_{ij}(z) = k_{ij}^b + \left(\frac{z}{h} + \frac{1}{2}\right)^n \left(k_{ij}^t - c_{ij}^b\right)
\end{aligned} \tag{11}$$

$$d_{ij}(z)=d_{ij}^{b}+\left(\frac{z}{h}+\frac{1}{2}\right)^{n}\left(d_{ij}^{t}-d_{ij}^{b}\right);\mu_{ij}(z)=\mu_{ij}^{b}+\left(\frac{z}{h}+\frac{1}{2}\right)^{n}\left(\mu_{ij}^{t}-\mu_{ij}^{b}\right)$$

where n is power index; $c_{ij}^{t},e_{ij}^{t},q_{ij}^{t},k_{ij}^{t},d_{ij}^{t},\mu_{ij}^{t}$ represent the material properties of the top side made of $CoFe_2O_4$ and $c_{ij}^{b},e_{ij}^{b},q_{ij}^{b},k_{ij}^{b},d_{ij}^{b},\mu_{ij}^{b}$ denote the material properties of the bottom side, which is made of $BaTiO_3$.

2.3. Variational principle

According to Hamilton's principle, the governing equation can be presented as follow

$$\delta U+\delta K-\delta V=0 \tag{12}$$

where δK and δU represent the virtual kinetic and strain energy, respectively; δW denotes the work done by the elastic foundation and initial external magnetic and electric loads.

The expression for the virtual strain energy δU is defined as follows

$$\delta U=\int_{V}\left(\delta\boldsymbol{\varepsilon}_b^{T}\boldsymbol{\sigma}_b+\delta\boldsymbol{\varepsilon}_s^{T}\boldsymbol{\sigma}_s-\delta\mathbf{E}_b^{T}\mathbf{D}_b-\delta\mathbf{E}_s^{T}\mathbf{D}_s-\delta\mathbf{H}_b^{T}\mathbf{B}_b-\delta\mathbf{H}_s^{T}\mathbf{B}_s\right)\mathrm{d}V \tag{13}$$

Inserting the appropriate expressions into Eq. (13) virtual strain energy is rewritten by

$$\begin{aligned}&\delta U=\int_{\Omega}\delta\bar{\boldsymbol{\varepsilon}}_b^{T}\bar{\mathbf{D}}_{uub}\bar{\boldsymbol{\varepsilon}}_b\mathrm{d}\Omega-\int_{\Omega}\delta\bar{\boldsymbol{\varepsilon}}_b^{T}\bar{\mathbf{D}}_{ueb}\bar{\mathbf{E}}_b\mathrm{d}\Omega-\int_{\Omega}\delta\bar{\boldsymbol{\varepsilon}}_b^{T}\bar{\mathbf{D}}_{umb}\bar{\mathbf{H}}^{b}\mathrm{d}\Omega+\int_{\Omega}\delta\boldsymbol{\gamma}_s^{T}\bar{\mathbf{D}}_{uus}\boldsymbol{\gamma}_s\mathrm{d}\Omega-\ldots\\&\int_{\Omega}\delta\boldsymbol{\gamma}_s^{T}\bar{\mathbf{D}}_{ues}\bar{\mathbf{E}}_s\mathrm{d}\Omega-\int_{\Omega}\delta\boldsymbol{\gamma}_s^{T}\bar{\mathbf{D}}_{ums}\bar{\mathbf{H}}_s\mathrm{d}\Omega-\int_{\Omega}\delta\bar{\mathbf{E}}_b^{T}\bar{\mathbf{D}}_{ueb}^{T}\bar{\boldsymbol{\varepsilon}}_b\mathrm{d}\Omega-\int_{\Omega}\delta\bar{\mathbf{E}}_b^{T}\bar{\mathbf{D}}_{eeb}\bar{\mathbf{E}}_b\mathrm{d}\Omega-\ldots\\&\int_{\Omega}\delta\bar{\mathbf{E}}_b^{T}\bar{\mathbf{D}}_{emb}\bar{\mathbf{H}}_b\mathrm{d}\Omega-\int_{\Omega}\delta\bar{\mathbf{E}}_s^{T}\bar{\mathbf{D}}_{ues}^{T}\boldsymbol{\gamma}_s\mathrm{d}\Omega-\int_{\Omega}\delta\bar{\mathbf{E}}_s^{T}\bar{\mathbf{D}}_{ees}\bar{\mathbf{E}}_s\mathrm{d}\Omega-\int_{\Omega}\delta\bar{\mathbf{E}}_s^{T}\bar{\mathbf{D}}_{ems}\bar{\mathbf{H}}_s\mathrm{d}\Omega-\ldots\\&\int_{\Omega}\delta\bar{\mathbf{H}}_b^{T}\bar{\mathbf{D}}_{umb}^{T}\bar{\boldsymbol{\varepsilon}}_b\mathrm{d}\Omega-\int_{\Omega}\delta\bar{\mathbf{H}}_b^{T}\bar{\mathbf{D}}_{emb}\bar{\mathbf{E}}_b\mathrm{d}\Omega-\int_{\Omega}\delta\bar{\mathbf{H}}_b^{T}\bar{\mathbf{D}}_{mmb}\bar{\mathbf{H}}_b\mathrm{d}\Omega-\int_{\Omega}\delta\bar{\mathbf{H}}_s^{T}\bar{\mathbf{D}}_{ums}^{T}\boldsymbol{\gamma}_s\mathrm{d}\Omega-\ldots\\&\int_{\Omega}\delta\bar{\mathbf{H}}_s^{T}\bar{\mathbf{D}}_{ems}\bar{\mathbf{E}}_s\mathrm{d}\Omega-\int_{\Omega}\delta\bar{\mathbf{H}}_s^{T}\bar{\mathbf{D}}_{mms}\bar{\mathbf{H}}_s\mathrm{d}\Omega\end{aligned} \tag{14}$$

where

$$\begin{aligned}&\bar{\mathbf{E}}_b=\begin{Bmatrix}0\\0\\-\varphi\end{Bmatrix};\bar{\mathbf{E}}_s=\begin{Bmatrix}-\varphi_{,x}\\-\varphi_{,y}\end{Bmatrix};\bar{\boldsymbol{\varepsilon}}_b=\begin{Bmatrix}\boldsymbol{\varepsilon}_{b1}\\\boldsymbol{\varepsilon}_{b2}\end{Bmatrix};\bar{\mathbf{H}}_b=\begin{Bmatrix}0\\0\\-\psi\end{Bmatrix};\bar{\mathbf{H}}_s=\begin{Bmatrix}-\psi_{,x}\\-\psi_{,y}\end{Bmatrix};\\&\bar{\mathbf{D}}_{uub}=\begin{bmatrix}\mathbf{A}_b&\mathbf{B}_b\\\mathbf{B}_b&\mathbf{D}_b\end{bmatrix};\bar{\mathbf{D}}_{uus}=\int_{-h/2}^{h/2}(1+f')^{2}\mathbf{C}_{uus}\mathrm{d}z;(\mathbf{A}_b,\mathbf{B}_b,\mathbf{D}_b)=\int_{-h/2}^{h/2}\left(z^{2},zf,f^{2}\right)\mathbf{C}_{uub}\mathrm{d}z;\\&\bar{\mathbf{D}}_{ueb}=\begin{Bmatrix}\mathbf{C}_{ueb}^{1}&\mathbf{C}_{ueb}^{2}\end{Bmatrix};\bar{\mathbf{D}}_{umb}=\begin{Bmatrix}\mathbf{C}_{umb}^{1}&\mathbf{C}_{umb}^{2}\end{Bmatrix};\left(\mathbf{C}_{ueb}^{1},\mathbf{C}_{ueb}^{2}\right)=\int_{-h/2}^{h/2}\mathbf{C}_{ueb}(z,f)g'\mathrm{d}z;\\&\left(\mathbf{C}_{umb}^{1},\mathbf{C}_{umb}^{2}\right)=\int_{-h/2}^{h/2}\mathbf{C}_{umb}(z,f)g'\mathrm{d}z;\bar{\mathbf{D}}_{ues}=\int_{-h/2}^{h/2}\mathbf{C}_{ues}(1+f')g\mathrm{d}z;\bar{\mathbf{D}}_{ums}=\int_{-h/2}^{h/2}\mathbf{C}_{ums}(1+f')g\mathrm{d}z;\\&\bar{\mathbf{D}}_{emb}=\int_{-h/2}^{h/2}\mathbf{C}_{emb}g'^{2}\mathrm{d}z;\bar{\mathbf{D}}_{ems}=\int_{-h/2}^{h/2}\mathbf{C}_{ems}g^{2}\mathrm{d}z;\bar{\mathbf{D}}_{eeb}=\int_{-h/2}^{h/2}\mathbf{C}_{eeb}g'^{2}\mathrm{d}z;\bar{\mathbf{D}}_{ees}=\int_{-h/2}^{h/2}\mathbf{C}_{ees}g^{2}\mathrm{d}z;\\&\bar{\mathbf{D}}_{mmb}=\int_{-h/2}^{h/2}\mathbf{C}_{mmb}g'^{2}\mathrm{d}z;\bar{\mathbf{D}}_{mms}=\int_{-h/2}^{h/2}\mathbf{C}_{mms}g^{2}\mathrm{d}z\end{aligned} \tag{15}$$

The virtual kinetic energy δK in Eq. (12) is given as follows

$$\delta K=\int_{\Omega}\delta\bar{\mathbf{u}}^{T}\mathbf{I}_m\ddot{\bar{\mathbf{u}}}\mathrm{d}\Omega \tag{16}$$

where

$$\bar{\mathbf{u}}=\begin{Bmatrix}\mathbf{u}_1\\\mathbf{u}_2\\\mathbf{u}_3\end{Bmatrix};\ \mathbf{I}_m=\begin{bmatrix}\mathbf{I}_0&0&0\\0&\mathbf{I}_0&0\\0&0&\mathbf{I}_0\end{bmatrix};\ \mathbf{I}_0=\begin{bmatrix}I_1&I_2&I_4\\I_2&I_3&I_5\\I_4&I_5&I_6\end{bmatrix};\qquad \left(I_1,I_2,I_3,I_4,I_5,I_6\right)=\int_{-h/2}^{h/2}\rho(z)\left(1,z,z^{2},f(z),zf(z),f^{2}(z)\right)\mathrm{d}z \tag{17}$$

The expression for the virtual work δW done by the external magnetic and electric loads and the elastic foundation is defined by

$$\delta W = \int_\Omega \delta \mathbf{N}_w^T \mathbf{N}_{em} \mathbf{N}_w \mathrm{d}\Omega - \int_\Omega \delta \tilde{w}\left(k_w \tilde{w} - k_s \nabla^2 \tilde{w}\right)\mathrm{d}\Omega;$$
$$\mathbf{N}_{em} = -\begin{bmatrix} 2\bar{e}_{31}V_0 + 2\bar{q}_{31}\Omega_0 & 0 \\ 0 & 2\bar{e}_{31}V_0 + 2\bar{q}_{31}\Omega_0 \end{bmatrix}; \mathbf{N}_w = \begin{Bmatrix} w_{b,x} + w_{s,x} \\ w_{b,y} + w_{s,y} \end{Bmatrix} \tag{18}$$

In the given context, the symbol k_s represents the shear coefficients of the foundation, while k_w denotes the spring coefficient of the foundation; ∇ denotes the gradient operator.

By inserting the Eqs. (14), (16) and (18) into Eq. (12), the governing equation of the FG MEE plate is reformed as follows

$$\begin{aligned}
&\int_\Omega \delta\bar{\boldsymbol{\varepsilon}}_b^T \bar{\mathbf{D}}_{uub} \bar{\boldsymbol{\varepsilon}}_b \mathrm{d}\Omega - \int_\Omega \delta\bar{\boldsymbol{\varepsilon}}_b^T \bar{\mathbf{D}}_{ueb} \bar{\mathbf{E}}_b \mathrm{d}\Omega - \int_\Omega \delta\bar{\boldsymbol{\varepsilon}}_b^T \bar{\mathbf{D}}_{umb} \bar{\mathbf{H}}^b \mathrm{d}\Omega + \int_\Omega \delta\boldsymbol{\gamma}_s^T \bar{\mathbf{D}}_{uus} \boldsymbol{\gamma}_s \mathrm{d}\Omega - ... \\
&\int_\Omega \delta\boldsymbol{\gamma}_s^T \bar{\mathbf{D}}_{ues} \bar{\mathbf{E}}_s \mathrm{d}\Omega - \int_\Omega \delta\boldsymbol{\gamma}_s^T \bar{\mathbf{D}}_{ums} \bar{\mathbf{H}}_s \mathrm{d}\Omega - \int_\Omega \delta\bar{\mathbf{E}}_b^T \bar{\mathbf{D}}_{ueb}^T \bar{\boldsymbol{\varepsilon}}_b \mathrm{d}\Omega - \int_\Omega \delta\bar{\mathbf{E}}_b^T \bar{\mathbf{D}}_{eeb} \bar{\mathbf{E}}_b \mathrm{d}\Omega - ... \\
&\int_\Omega \delta\bar{\mathbf{E}}_b^T \bar{\mathbf{D}}_{emb} \bar{\mathbf{H}}_b \mathrm{d}\Omega - \int_\Omega \delta\bar{\mathbf{E}}_s^T \bar{\mathbf{D}}_{ues}^T \boldsymbol{\gamma}_s \mathrm{d}\Omega - \int_\Omega \delta\bar{\mathbf{E}}_s^T \bar{\mathbf{D}}_{ees} \bar{\mathbf{E}}_s \mathrm{d}\Omega - \int_\Omega \delta\bar{\mathbf{E}}_s^T \bar{\mathbf{D}}_{ems} \bar{\mathbf{H}}_s \mathrm{d}\Omega - ... \\
&\int_\Omega \delta\bar{\mathbf{H}}_b^T \bar{\mathbf{D}}_{umb}^T \bar{\boldsymbol{\varepsilon}}_b \mathrm{d}\Omega - \int_\Omega \delta\bar{\mathbf{H}}_b^T \bar{\mathbf{D}}_{emb} \bar{\mathbf{E}}_b \mathrm{d}\Omega - \int_\Omega \delta\bar{\mathbf{H}}_b^T \bar{\mathbf{D}}_{mmb} \bar{\mathbf{H}}_b \mathrm{d}\Omega - \int_\Omega \delta\bar{\mathbf{H}}_s^T \bar{\mathbf{D}}_{ums}^T \boldsymbol{\gamma}_s \mathrm{d}\Omega - ... \\
&\int_\Omega \delta\bar{\mathbf{H}}_s^T \bar{\mathbf{D}}_{ems} \bar{\mathbf{E}}_s \mathrm{d}\Omega - \int_\Omega \delta\bar{\mathbf{H}}_s^T \bar{\mathbf{D}}_{mms} \bar{\mathbf{H}}_s \mathrm{d}\Omega + \int_\Omega \delta\tilde{w}\left(k_w \tilde{w} - k_s \nabla^2 \tilde{w}\right)\mathrm{d}\Omega - \int_\Omega \delta\mathbf{N}_w^T \mathbf{N}_{em} \mathbf{N}_w \mathrm{d}\Omega \\
&+ \int_\Omega \delta\bar{\mathbf{u}}^T \mathbf{I}_m \ddot{\bar{\mathbf{u}}} \mathrm{d}\Omega = 0
\end{aligned} \tag{19}$$

2.4. The NURBS approximation

Employing the NURBS basis functions [14], the vector of displacement $\mathbf{u}$, magnetic potential ψ, and electric potential φ are approximated by

$$\mathbf{u}(x,y) = \sum_{I=1}^{m\times n} \mathbf{N}_I(x,y)\mathbf{q}_I;\ \psi(x,y) = \sum_{I=1}^{m\times n} \mathbf{N}_{\psi I}(x,y)\boldsymbol{\chi}_I;\ \varphi(x,y) = \sum_{I=1}^{m\times n} \mathbf{N}_{\varphi I}(x,y)\boldsymbol{\chi}_I \tag{20}$$

where

$$\mathbf{N}_I(x,y) = \begin{bmatrix} N_I(x,y) & 0 \\ 0 & N_I(x,y) \end{bmatrix}; \mathbf{N}_{\psi I}(x,y) = \begin{Bmatrix} 0 & N_I(x,y) \end{Bmatrix}; \mathbf{N}_{\varphi I}(x,y) = \begin{Bmatrix} N_I(x,y) & 0 \end{Bmatrix};$$
$$\mathbf{q}_I = \begin{Bmatrix} w_{bI} & w_{sI} \end{Bmatrix}^T; \boldsymbol{\chi}_I = \begin{Bmatrix} \varphi_I & \psi_I \end{Bmatrix}^T \tag{21}$$

in which $N_I(x,y)$ denotes the NURBS basic function.

The linear strain, magnetic and electric fields are rewritten after the inserting Eq. (20) into Eq. (15) as follows

$$\begin{aligned}
&\bar{\boldsymbol{\varepsilon}}_b = \sum_{I=1}^{m\times n} \begin{Bmatrix} \bar{\mathbf{B}}_{b1I} \\ \bar{\mathbf{B}}_{b2I} \end{Bmatrix} \mathbf{q}_I = \sum_{I=1}^{m\times n} \bar{\mathbf{B}}_{bI}\mathbf{q}_I;\ \boldsymbol{\gamma}_s = \sum_{I=1}^{m\times n} \bar{\mathbf{B}}_{sI}\mathbf{d}_I; \\
&\bar{\mathbf{E}}_b = \sum_{I=1}^{m\times n} \bar{\mathbf{B}}_{\varphi bI}\boldsymbol{\chi}_I;\ \bar{\mathbf{E}}_s = \sum_{I=1}^{m\times n} \bar{\mathbf{B}}_{\varphi sI}\boldsymbol{\chi}_I;\ \bar{\mathbf{H}}_b = \sum_{I=1}^{m\times n} \bar{\mathbf{B}}_{\psi bI}\boldsymbol{\chi}_I;\ \bar{\mathbf{H}}_s = \sum_{I=1}^{m\times n} \bar{\mathbf{B}}_{\psi sI}\boldsymbol{\chi}_I
\end{aligned} \tag{22}$$

in which

$$\mathbf{B}_{b1I} = -\begin{bmatrix} N_{I,xx} & 0 \\ N_{I,yy} & 0 \\ 2N_{I,xy} & 0 \end{bmatrix}; \mathbf{B}_{b2I} = \begin{bmatrix} 0 & N_{I,xx} \\ 0 & N_{I,yy} \\ 0 & 2N_{I,xy} \end{bmatrix}; \bar{\mathbf{B}}_{sI} = \begin{bmatrix} 0 & N_{I,x} \\ 0 & N_{I,y} \end{bmatrix}; \bar{\mathbf{B}}_{\varphi bI} = \begin{bmatrix} 0 & 0 \\ 0 & 0 \\ -N_I & 0 \end{bmatrix};$$
$$\bar{\mathbf{B}}_{\psi bI} = \begin{bmatrix} 0 & 0 \\ 0 & 0 \\ 0 & -N_I \end{bmatrix}; \bar{\mathbf{B}}_{\varphi sI} = \begin{bmatrix} -N_{I,x} & 0 \\ -N_{I,y} & 0 \end{bmatrix}; \bar{\mathbf{B}}_{\psi sI} = \begin{bmatrix} 0 & -N_{I,x} \\ 0 & -N_{I,y} \end{bmatrix} \tag{23}$$

The vector $\ddot{\bar{\mathbf{u}}}$ in Eq. (16) according to Eq. (20) is reformed by

$$\bar{\mathbf{u}} = \begin{Bmatrix} \mathbf{u}_1 \\ \mathbf{u}_2 \\ \mathbf{u}_3 \end{Bmatrix} = \sum_{I=1}^{m\times n} \begin{Bmatrix} \mathbf{N}_{1I} \\ \mathbf{N}_{2I} \\ \mathbf{N}_{3I} \end{Bmatrix} \mathbf{q}_I = \sum_{I=1}^{m\times n} \bar{\mathbf{N}}_I \mathbf{q}_I \tag{24}$$

where

$$\mathbf{N}_{1I} = \begin{bmatrix} 0 & 0 \\ 0 & 0 \\ N_I & N_I \end{bmatrix}; \mathbf{N}_{2I} = \begin{bmatrix} -N_{I,x} & 0 \\ -N_{I,y} & 0 \\ 0 & 0 \end{bmatrix}; \mathbf{N}_{3I} = \begin{bmatrix} 0 & N_{I,x} \\ 0 & N_{I,y} \\ 0 & 0 \end{bmatrix} \tag{25}$$

By the substituting Eq. (20) into Eq. (18), the vectors $\mathbf{N}_w$ can be reformed as follows

$$\mathbf{N}_w = \sum_{I=1}^{m\times n} \bar{\mathbf{B}}_{wI} \mathbf{q}_I ; \bar{\mathbf{B}}_{wI} = \begin{bmatrix} N_{I,x} & N_{I,x} \\ N_{I,y} & N_{I,y} \end{bmatrix} \tag{26}$$

By substituting Eqs. (22), (24) and (26) into Eq. (19), the weak form for free vibration analysis of the FG MEE plate is presented by following

$$\left(\mathbf{K} - \omega^2 \mathbf{M}\right)\tilde{\mathbf{q}} = 0 \tag{27}$$

where

$$\begin{aligned}
&\mathbf{K} = \mathbf{K}_{uu} - \mathbf{K}_{u\chi}\mathbf{K}_{\chi\chi}^{-1}\mathbf{K}\mathbf{K}_{u\chi}^T; \\
&\mathbf{K}_{uu} = \int_\Omega \bar{\mathbf{B}}_b^T \bar{\mathbf{D}}_{uub} \bar{\mathbf{B}}_b \mathrm{d}\Omega + \int_\Omega \bar{\mathbf{B}}_s^T \bar{\mathbf{D}}_{uus} \bar{\mathbf{B}}_s \mathrm{d}\Omega + \int_\Omega \mathbf{B}_F^T \left(k_w \mathbf{B}_F - k_s \nabla^2 \mathbf{B}_F\right)\mathrm{d}\Omega - \int_\Omega \mathbf{B}_w^T \mathbf{N}_{em} \mathbf{B}_w \mathrm{d}\Omega; \\
&\mathbf{K}_{u\chi} = -\int_\Omega \bar{\mathbf{B}}_b^T \bar{\mathbf{D}}_{ueb} \bar{\mathbf{B}}_{\varphi b} \mathrm{d}\Omega - \int_\Omega \bar{\mathbf{B}}_s^T \bar{\mathbf{D}}_{ues} \bar{\mathbf{B}}_{\varphi s} \mathrm{d}\Omega - \int_\Omega \bar{\mathbf{B}}_b^T \bar{\mathbf{D}}_{umb} \bar{\mathbf{B}}_{\psi b} \mathrm{d}\Omega - \int_\Omega \bar{\mathbf{B}}_s^T \bar{\mathbf{D}}_{ums} \bar{\mathbf{B}}_{\psi s} \mathrm{d}\Omega; \\
&\mathbf{K}_{\chi\chi} = -\int_\Omega \bar{\mathbf{B}}_{\varphi b}^T \bar{\mathbf{D}}_{eeb} \bar{\mathbf{B}}_{\varphi b} \mathrm{d}\Omega - \int_\Omega \bar{\mathbf{B}}_{\varphi s}^T \bar{\mathbf{D}}_{ees} \bar{\mathbf{B}}_{\varphi s} \mathrm{d}\Omega - \int_\Omega \bar{\mathbf{B}}_{\varphi b}^T \bar{\mathbf{D}}_{emb} \bar{\mathbf{B}}_{\psi b} \mathrm{d}\Omega - \int_\Omega \bar{\mathbf{B}}_{\varphi s}^T \bar{\mathbf{D}}_{ems} \bar{\mathbf{B}}_{\psi s} \mathrm{d}\Omega - ... \\
&\int_\Omega \bar{\mathbf{B}}_{\psi b}^T \bar{\mathbf{D}}_{emb} \bar{\mathbf{B}}_{\varphi b} \mathrm{d}\Omega - \int_\Omega \bar{\mathbf{B}}_{\psi s}^T \bar{\mathbf{D}}_{ems} \bar{\mathbf{B}}_{\varphi s} \mathrm{d}\Omega - \int_\Omega \bar{\mathbf{B}}_{\psi b}^T \bar{\mathbf{D}}_{mmb} \bar{\mathbf{B}}_{\psi b} \mathrm{d}\Omega - \int_\Omega \bar{\mathbf{B}}_{\psi s}^T \bar{\mathbf{D}}_{mms} \bar{\mathbf{B}}_{\psi s} \mathrm{d}\Omega; \\
&\mathbf{M} = \int_\Omega \bar{\mathbf{N}}^T \mathbf{I}_m \bar{\mathbf{N}} \mathrm{d}\Omega; \mathbf{q} = \tilde{\mathbf{q}} \mathrm{e}^{i\omega t}; \mathbf{B}_F = \begin{Bmatrix} N_I & N_I \end{Bmatrix}
\end{aligned} \tag{28}$$

where $\mathbf{M}$ is the mass matrix; ω represents natural frequency; $\tilde{\mathbf{q}}$ denotes the mode shape.

3. Numerical results

In this section, the FG MEE rectangular and circular plates with various boundary conditions (BCs) are studied. The Dirichlet BCs of the rectangular plate are presented as follows

- Fully simply supported (SSSS): $w_b\big|_{x=0,a;y=0,b} = w_s\big|_{x=0,a;y=0,b} = 0$
- Fully clamped (CCCC): $\begin{cases} w_b\big|_{x=0,a;y=0,b} = w_s\big|_{x=0,a;y=0,b} = 0 \\ w_{b,n}\big|_{x=0,a;y=0,b} = w_{s,n}\big|_{x=0,a;y=0,b} = 0 \end{cases}$

In addition, the BCs of the circular are taken by

- Simply supported (SS): $w_b = w_s = 0$ at the boundary
- Clamped (CC): $w_b = w_s = w_{b,n} = w_{s,n} = 0$ at the boundary

Firstly, the free vibration response of the homogeneous MEE square plate with the material properties given in Table 1 is investigated to validate the accuracy and consistency of the present model. The plate is modelled by 7×7, 9×9, 11×11 and 13×13 cubic NURBS elements. The first three non-dimensional natural frequencies $\hat{\omega} = \omega a\sqrt{\rho/\bar{c}_{11}}$ of the SSSS homogeneous MEE square plate are presented in Table 2. The frequencies are compared with those given by Abazid et al. [25], Glohami et al. [26] and Ke et al. [27]. Upon reviewing Table 2, it is evident that the numerical results obtained using the presented method closely align with those provided in the literature. Besides, it is apparent that the disparity between the mesh levels is inconsequential. Therefore, the mesh 11×11 elements will be utilized for the subsequent analysis. The comparison results in Table 2 indicate that the proposed model is accurate and

consistent.

Subsequently, novel findings regarding the free vibration analysis of FG MEE plates resting on a Winkler-Pasternak foundation, considering the material properties given in Table 3, are presented. Besides, the following dimensionless quantities are used during the numerical calculation

$$K_w = \frac{k_w a^4}{\bar{c}_{11} h^3}; K_s = \frac{k_s a^2}{\bar{c}_{11} h^3}; \phi_0 = \frac{100 V_0 a}{\bar{c}_{11} h^3}; \psi_0 = \frac{100 \Omega_0 a}{\bar{c}_{11} h^3} \quad (29)$$

The influence of the power index n on the first five normalized natural frequencies $\bar{\omega}$ of the FG MEE rectangular plates resting on an elastic foundation with various values of the with-to-length ratio b/a is explored in Table 4. Based on the results in Table 4, by raising the power index, the frequencies of the FG MEE rectangular plates reduce. That is because cobalt ferrite ($CoFe_2O_4$) content in the FG MEE rectangular plate decreased with the growth of the parameter n resulting in a decrease in the plate's stiffness. Besides, expanding the parameter b/a leads to a reduced frequency FG MEE rectangular plate. In addition, the CCCC FG MEE rectangular plate provides a higher frequency than the SSSS rectangular plate. Besides, Figure 2 illustrates the impact of the normalized external electric voltage ϕ_0 and magnetic potential ψ_0 on the first natural frequency $\bar{\omega}$ of the SSSS and CCCC FG MEE square plates. It can be observed from Figure 2 that the growth of the parameters ϕ_0 and ψ_0 make the vibration frequency of the FG MEE plates decrease and increase, respectively.

Moreover, the impact of the normalized spring coefficient K_w on the first non-dimensional natural frequency $\bar{\omega}$ is tabulated in Table 5, while the influence of the normalized shear coefficient K_s on the first normalized frequency $\bar{\omega}$ of the FG MEE square plate is presented in Table 6. The impact of the length-to-thickness ratio a/h on the first frequency of the FG MEE square plates is also shown in these tables. According to Table 5 and Table 6, the FG MEE plate becomes stiffer with the rise of the coefficients K_w and K_s of the Winkler-Pasternak foundation. Meanwhile, the stiffness of the FG MEE plate decreases with increasing the length-to-thickness ratio. The first four mode shapes of the SSSS FG MEE square plate are also plotted in Figure 2. Finally, the first five dimensionless natural frequencies $\breve{\omega} = \omega R\sqrt{\rho/\bar{c}_{11}}$ of the simply supported (SS) and clamped (CC) FG MEE circular plates with various values of the power index are presented in Table 7. According to Table 7, the dimensionless natural frequencies of the FG MEE circular plate decrease with an increase in the parameter n.

Table 1. *Material properties of the homogeneous MEE plate.*

Properties	**$BaTiO_3$-$CoFe_2O_4$**
Elastic (GPa)	$c_{11} = c_{22} = 226; c_{12} = 125; c_{13} = 124; c_{44} = c_{55} = 44.2; c_{66} = 50.5$
Piezoelectric (C/m^2)	$e_{31} = e_{32} = -2.2; e_{33} = 9.3; e_{15} = 5.8$
Dielectric (10^{-9} C/V.m)	$k_{11} = k_{22} = 5.64; k_{33} = 6.35$
Piezomagnetic (N/A.m)	$q_{15} = q_{24} = 275; q_{31} = q_{32} = 290.1; q_{33} = 349.9$
Magnetoelectric (10^{-12} Ns/VC)	$d_{11} = d_{22} = 5.367; d_{33} = 2737.5$
Magnetic (10^{-6} Ns^2/C^2)	$\mu_{11} = \mu_{22} = -297; \mu_{33} = 83.5$
Density (kg/m^3)	$\rho = 5550$

Table 2. *The first three non-dimensional natural frequencies $\bar{\omega}$ of a SSSS MEE square plates ($a = b = 15h$; $\phi_0 = \psi_0 = 0$).*

Theory	**Meshes**	**Mode**		
		1	2	4
Ref [25]		0.3698	0.9247	1.4568
Ref [26]		0.3682	0.9136	-
Ref [27]		0.3698	0.9247	1.4800
Present	7×7	0.3830	0.9333	1.4574

9×9	0.3830	0.9331	1.4572
11×11	0.3830	0.9330	1.4571
13×13	0.3829	0.9330	1.4571

Table 3. *The material properties of the FG MEE plates.*

Properties	Bottom ($BaTiO_3$)	Top ($CoFe_2O_4$)
Elastic (GPa)	$c_{11}=c_{22}=166; c_{33}=162; c_{12}=77;$ $c_{13}=c_{23}=78; c_{55}=43; c_{66}=44.5$	$c_{11}=c_{22}=286; c_{33}=269.5;$ $c_{12}=173; c_{13}=c_{23}=170.5;$ $c_{55}=45.3; c_{66}=56.5$
Piezoelectric (C/m^2)	$e_{31}=-4.4; e_{33}=18.6; e_{15}=11.6$	$e_{31}=0; e_{33}=0; e_{15}=0$
Dielectric (10^{-9} C/V.m)	$k_{11}=k_{22}=11.2; k_{33}=12.6$	$k_{11}=k_{22}=0.08; k_{33}=0.093$
Piezomagnetic (N/A.m)	$q_{31}=q_{33}=q_{15}=0$	$q_{31}=580.3; q_{33}=699.7; q_{15}=550$
Magnetoelectric (10^{-12} Ns/VC)	$d_{11}=d_{22}=d_{33}=0$	$d_{11}=d_{22}=d_{33}=0$
Magnetic (10^{-6} Ns^2/C^2)	$\mu_{11}=\mu_{22}=5; \mu_{33}=10$	$\mu_{11}=\mu_{22}=-590; \mu_{33}=157$
Density (kg/m^3)	$\rho=5800$	$\rho=5300$

Table 4. *The first five natural frequencies of the FG MEE rectangular plate with different power indexes and width-to-length ratios (a/h = 10, K_w = 1, K_s = 0.1, ϕ_0 = ψ_0 = 0).*

BCs	Mode	b/a =1				b/a =2			
		n				n			
		1	2	5	10	1	2	5	10
SSSS	1	0.5365	0.5281	0.5217	0.5200	0.3544	0.3490	0.3447	0.3436
	2	1.2315	1.2139	1.2007	1.1977	0.5364	0.5281	0.5217	0.5199
	3	1.2315	1.2139	1.2007	1.1977	0.8336	0.8209	0.8112	0.8088
	4	1.8690	1.8448	1.8274	1.8243	1.0636	1.0479	1.0361	1.0333
	5	2.2674	2.2400	2.2208	2.2180	1.2315	1.2138	1.2006	1.1976
CCCC	1	0.8919	0.8795	0.8704	0.8685	0.6304	0.6212	0.6144	0.6128
	2	1.6966	1.6763	1.6618	1.6601	0.8069	0.7951	0.7863	0.7844
	3	1.6966	1.6763	1.6618	1.6601	1.1064	1.0908	1.0792	1.0769
	4	2.3790	2.3529	2.3356	2.3349	1.5036	1.4845	1.4710	1.4691
	5	2.7676	2.7421	2.7264	2.7278	1.5141	1.4940	1.4794	1.4769

Table 5. *The impact of the normalized spring coefficient K_w of the foundation of the FG MEE square plate with various length-to-thickness ratios (n = 2, ϕ_0 =1, ψ_0= 0.02, K_s = 0.1).*

BCs	a/h	K_w				
		0	0.5	1	1.5	2
SSSS	10	0.5273	0.5317	0.5360	0.5404	0.5447
	20	0.2706	0.2728	0.2749	0.2770	0.2791
	30	0.1813	0.1827	0.1842	0.1856	0.1870
CCCC	10	0.8798	0.8825	0.8851	0.8877	0.8903

	20	0.4710	0.4723	0.4735	0.4747	0.4760
	30	0.3185	0.3193	0.3201	0.3209	0.3217

Table 6. *The impact of the normalized shear coefficient K_s of the foundation of the FG MEE square plate with various length-to-thickness ratios (n = 2, ϕ_0 =1, ψ_0 = 0.02, K_w = 1).*

BCs	***a*/*h***	***Ks***				
		0	0.05	0.1	0.15	0.2
SSSS	10	0.5186	0.5274	0.5360	0.5445	0.5529
	20	0.2663	0.2706	0.2749	0.2791	0.2832
	30	0.1785	0.1814	0.1842	0.1870	0.1897
CCCC	10	0.8728	0.8790	0.8851	0.8912	0.8972
	20	0.4676	0.4705	0.4735	0.4764	0.4793
	30	0.3162	0.3181	0.3201	0.3220	0.3240

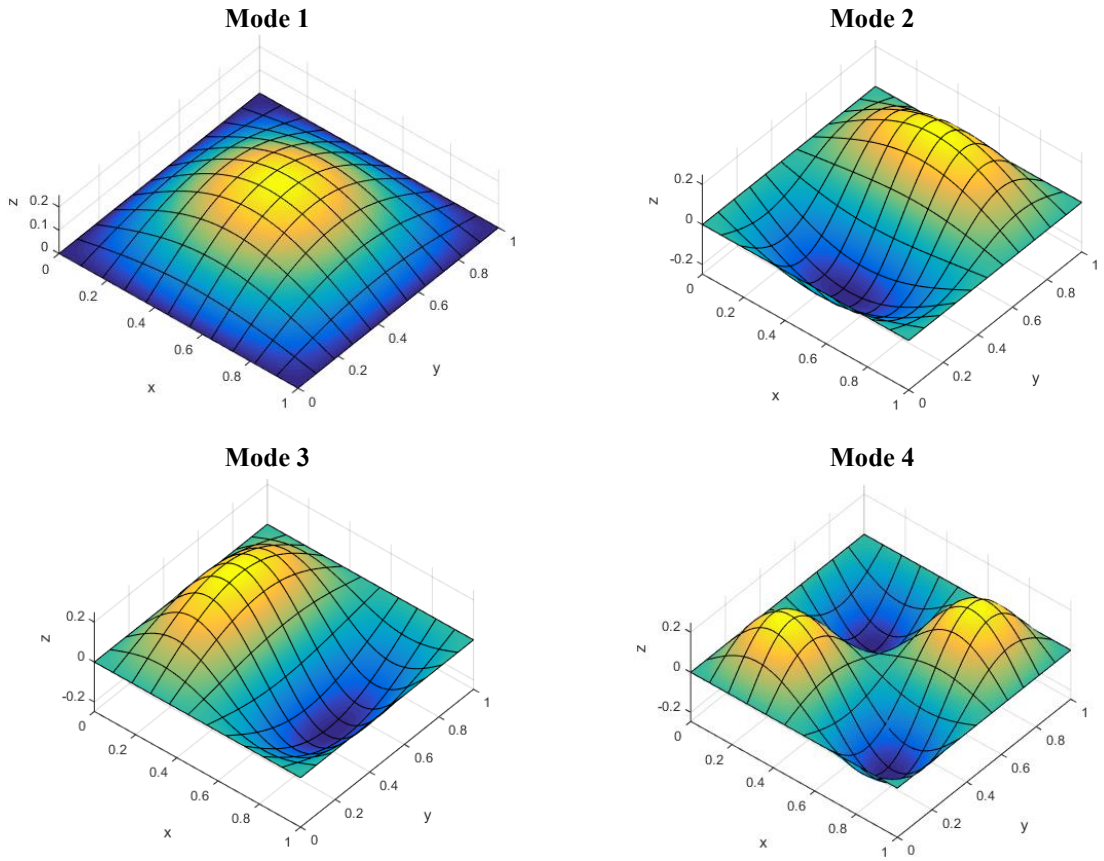

Figure 2. *The first four mode shapes of the SSSS FG MEE square plate (a/h =10, n = 5, ϕ_0 = 1, ψ_0 = 0.01, K_w = 1, K_s = 0.1).*

Table 7. *The first five natural frequencies $\bar{\omega}$ of the FG MEE circular plate with different power indexes (R =1, R/h = 10, K_w = K_s = 0, ϕ_0 = ψ_0 = 0).*

Mode	**BCs**	
	SS	**CC**
	n	***n***

	1	2	5	10	1	2	5	10
1	0.1340	0.1316	0.1298	0.1292	0.2661	0.2617	0.2582	0.2573
2	0.3655	0.3592	0.3544	0.3530	0.5417	0.5331	0.5264	0.5247
3	0.3655	0.3592	0.3544	0.3530	0.5417	0.5331	0.5264	0.5247
4	0.6566	0.6460	0.6378	0.6357	0.8659	0.8528	0.8430	0.8407
5	0.6567	0.6461	0.6380	0.6358	0.8671	0.8540	0.8441	0.8418

4. Conclusions

The free vibration of the FG MEE plates resting on an elastic foundation using the RPT with two variables and IGA was investigated in this paper. Governing equations are derived with the help of the RPT and Hamilton's principle. The NURBS basic functions of the IGA approximate the plate's displacement, electric and magnetic fields. The validity of the current method has been established by comparing it with prior references, thereby confirming its accuracy and reliability. The impact of the power index, the coefficients of an elastic foundation, initial external electric and magnetic loads, and the geometries on the natural frequencies of the FG MEE plates is presented and discussed. The numerical results obtained from this article show that an increase in the power index reduces the stiffness of the FG MEE plate. Increasing the initial external electric voltage decreases the natural frequency of FG MEE plates while increasing the initial external magnetic potential increases it. Besides, the FG MEE plate becomes stiffer regarding the rise of the spring and shear coefficients of an elastic foundation. Finally, FG MEE plates become softer as their width-to-length and length-to-thickness ratios increase.

Acknowledgment

This work belongs to the project in 2023 funded by Ho Chi Minh City University of Technology and Education, Vietnam.

Conflict of Interest

The authors declare that they have no known competing financial interests or personal relationships that could have appeared to influence the work reported in this paper.

REFERENCES

[1] E. Pan, "Exact solution for simply supported and multilayered magneto-electro-elastic plates," *J. Appl. Mech.*, vol. 68, pp. 608-618, 2001.
[2] F. Ramirez, P. R. Heyliger, and E. Pan, "Free vibration response of two-dimensional magneto-electro-elastic laminated plates," *Journal of Sound and Vibration*, vol. 292, pp. 626-644, 2006.
[3] J. M. S. Moita, C. M. M. Soares, and C. A. M. Soares, "Analyses of magneto-electro-elastic plates using a higher order finite element model," *Composite structures*, vol. 91, pp. 421-426, 2009.
[4] T. M. Badri and H. H. Al-Kayiem, "Analytical solution for simply supported and multilayered magneto-thermo-electro-elastic plates," *Asian journal of scientific research*, vol. 6, pp. 236-244, 2012.
[5] M. Vinyas and D. Harursampath, "Computational evaluation of electro-magnetic circuits' effect on the coupled response of multifunctional magneto-electro-elastic composites plates exposed to hygrothermal fields," *Proceedings of the Institution of Mechanical Engineers, Part C: Journal of Mechanical Engineering Science*, vol. 235, pp. 2832-2850, 2021.
[6] A. Shooshtari and S. Razavi, "Large amplitude free vibration of symmetrically laminated magneto-electro-elastic rectangular plates on Pasternak type foundation," *Mechanics Research Communications*, vol. 69, pp. 103-113, 2015.
[7] M. Malikan and V. B. Nguyen, "Buckling analysis of piezo-magnetoelectric nanoplates in hygrothermal environment based on a novel one variable plate theory combining with higher-order nonlocal strain gradient theory," *Physica E: Low-dimensional Systems and Nanostructures*, vol. 102, pp. 8-28, 2018.
[8] C. P. Wu, S. J. Chen, and K. H. Chiu, "Three-dimensional static behavior of functionally graded magneto-electro-elastic plates using the modified Pagano method," *Mechanics Research Communications*, vol. 37, pp. 54-60, 2010.
[9] C. P. Wu and Y. C. Lu, "A modified Pagano method for the 3D dynamic responses of functionally graded magneto-electro-elastic plates," *Composite Structures*, vol. 90, pp. 363-372, 2009.
[10] F. Ebrahimi and A. Jafari, "Buckling behavior of smart MEE-FG porous plate with various boundary conditions based on refined theory," *Advances in materials Research*, vol. 5, p. 279, 2016.
[11] Y. Ni *et al.*, "An accurate model for free vibration of porous magneto-electro-thermo-elastic functionally graded cylindrical shells subjected to multi-field coupled loadings," *Journal of Intelligent Material Systems and Structures*, vol. 32, pp. 2006-2023, 2021.
[12] J. Sladek, V. Sladek, S. Krahulec, C. Chen, and D. Young, "Analyses of circular magnetoelectroelastic plates with functionally graded material properties," *Mechanics of Advanced Materials and Structures*, vol. 22, pp. 479-489, 2015.
[13] F. Ebrahimi, N. Farazmandnia, M. R. Kokaba, and V. Mahesh, "Vibration analysis of porous magneto-electro-elastically actuated carbon nanotube-reinforced composite sandwich plate based on a refined plate theory," *Engineering with Computers*, vol. 37, pp. 921-936, 2021.
[14] T. J. Hughes, J. A. Cottrell, and Y. Bazilevs, "Isogeometric analysis: CAD, finite elements, NURBS, exact geometry and mesh refinement," *Computer methods in applied mechanics and engineering*, vol. 194, pp. 4135-4195, 2005.

[15] H. Pham-Tan, C. H. Thai, and P. Phung-Van, "NURBS-based refined plate theory for metal foam plates with porosities," *Th in-Walled Structures*, vol. 175, p. 109246, 2022.
[16] P. Phung-Van, C. H. Thai, A. J. M. Ferreira, and T. Rabczuk, "Isogeometric nonlinear transient analysis of porous FGM pla tes subjected to hygro-thermo-mechanical loads," *Thin-Walled Structures*, vol. 148, p. 106497, 2020.
[17] C. H. Thai, A. J. M. Ferreira, and P. Phung-Van, "Free vibration analysis of functionally graded anisotropic microplates usi ng modified strain gradient theory," *Engineering Analysis with Boundary Elements*, vol. 117, pp. 284-298, 2020.
[18] C. H. Thai, A. J. M. Ferreira, and P. P. Van, "Size dependent free vibration analysis of multilayer functionally graded GPL RC microplates based on modified strain gradient theory," *Composites Part B: Engineering*, vol. 169, pp. 174-188, 2019.
[19] C. H. Thai, A. J. M. Ferreira, H. N. Xuan, and P. P. Van, "A size dependent meshfree model for functionally graded plate s based on the nonlocal strain gradient theory," *Composite Structures*, vol. 272, p. 114169, 2021.
[20] P. Phung-Van, A. J. M. Ferreira, H. Nguyen-Xuan, and C. H. Thai, "A nonlocal strain gradient isogeometric nonlinear analy sis of nanoporous metal foam plates," *Engineering Analysis with Boundary Elements*, vol. 130, pp. 58-68, 2021.
[21] R. P. Shimpi, "Refined plate theory and its variants," *AIAA journal*, vol. 40, pp. 137-146, 2002.
[22] L. L. Ke and Y. S. Wang, "Free vibration of size-dependent magneto-electro-elastic nanobeams based on the nonlocal theor y," *Physica E: Low-Dimensional Systems and Nanostructures*, vol. 63, pp. 52-61, 2014.
[23] A. Jamalpoor, A. Ahmadi-Savadkoohi, M. Hosseini, and S. Hosseini-Hashemi, "Free vibration and biaxial buckling analysis of double magneto-electro-elastic nanoplate-systems coupled by a visco- Pasternak medium via nonlocal elasticity theory," *E uropean Journal of Mechanics - A/Solids*, vol. 63, pp. 84-98, 2017.
[24] F. Ebrahimi and M. R. Barati, "Vibration analysis of embedded biaxially loaded magneto-electrically actuated inhomogeneous nanoscale plates," *Journal of Vibration and Control*, vol. 24, pp. 3587-3607, 2018.
[25] M. A. Abazid, "The nonlocal strain gradient theory for hygrothermo-electromagnetic effects on buckling, vibration and wave propagation in piezoelectromagnetic nanoplates," *International Journal of Applied Mechanics*, vol. 11, p. 1950067, 2019.
[26] R. Gholami, R. Ansari, and Y. Gholami, "Size-dependent bending, buckling and vibration of higher-order shear deformable magneto-electro-thermo-elastic rectangular nanoplates," *Materials Research Express*, vol. 4, p. 065702, 2017.
[27] L. L. Ke, Y. S. Wang, J. Yang, and S. Kitipornchai, "Free vibration of size-dependent magneto-electro-elastic nanoplates bas ed on the nonlocal theory," *Acta Mechanica Sinica*, vol. 30, pp. 516-525, 2014.

L. T. Phong was born in Vietnam in 1971. He has a Master. degree in Mechanics. Now, he is a lecturer at the Faculty of Civil Engineering at Ho Chi Minh City University of Technology and Education, Ho Chi Minh City, Vietnam. His research interests are the computational mechanics. Email address: phonglt@hcmute.edu.vn.

T. Nguyen-Thanh was born in Vietnam in 1987. He has a M.EnG in Civil Engineering. Now, he is working at the Faculty of Civil Engineering at Ho Chi Minh City University of Technology (HUTECH University), Ho Chi Minh City, Vietnam. Email: nguyenthanhtrung.ce@gmail.com

N. A. Dat was born in Vietnam in 1981. He has a Civil Engineering from Ho Chi Minh City University Artchitecture in 2011. Now, he is working at the Phu Minh Cuong Construction Company Limited, Ho Chi Minh City, Vietnam. Email: 2080802@student.hcmute.edu.vn

T. T. Trien was born in Vietnam in 1982. He has a Master. degree in Mechanics. Now, he is a lecturer at the Faculty of Civil Engineering at Ho Chi Minh City University of Technology and Education, Ho Chi Minh City, Vietnam. His research interests are the computational mechanics. Email address: trientt@hcmute.edu.vn.

P. T. Hung was born in Vietnam in 1981. He has a Ph.D. degree in Mechanics. Now, he is a lecturer at the Faculty of Civil Engineering at Ho Chi Minh City University of Technology and Education, Ho Chi Minh City, Vietnam. His research interests are the computational mechanics. Email: hungpht@hcmute.edu.vn.
ORCID: https://orcid.org/0000-0001-6105-9311